BIOMIMETICS

Kirigami skins make a simple soft actuator crawl

Ahmad Rafsanjani, Yuerou Zhang, Bangyuan Liu, Shmuel M. Rubinstein, Katia Bertoldi*

Bioinspired soft machines made of highly deformable materials are enabling a variety of innovative applications, yet their locomotion typically requires several actuators that are independently activated. We harnessed kirigami principles to significantly enhance the crawling capability of a soft actuator. We designed highly stretchable kirigami surfaces in which mechanical instabilities induce a transformation from flat sheets to 3D-textured surfaces akin to the scaled skin of snakes. First, we showed that this transformation was accompanied by a dramatic change in the frictional properties of the surfaces. Then, we demonstrated that, when wrapped around an extending soft actuator, the buckling-induced directional frictional properties of these surfaces enabled the system to efficiently crawl.

INTRODUCTION

Nature offers many examples of slender limbless organisms that take advantage of both the flexibility of their body and the frictional properties of their skin to efficiently move and explore the surrounding space (*1*–*5*). For example, snakes rely on the substantial reconfiguration in the shape of their body (*6*) and on the frictional anisotropy of their skin (*7*) to propel themselves. Not only microscopic features (*8*, *9*) but also the macroscale structure and arrangement of their ventral scales contribute to such anisotropic friction (*5*), because their preferred orientation makes sliding in the forward direction much easier than in the backward one.

The flexibility of soft-bodied animals has recently inspired the design of new class of soft robots that are easy and inexpensive to fabricate yet still can achieve complex motions (*10*–*14*). However, efforts to replicate natural frictional properties in synthetic systems have been limited (*15*, *16*). The skin of the vast majority of soft robots consists of an unstructured flexible membrane that lacks directional frictional properties. As a result, multiple actuators activated independently are typically required to achieve locomotion (*16*–*21*).

Inspired by the friction-assisted locomotion of snakes (*1*, *5*, *7*) and by the recent advances in engineered surfaces with programmable tribological behavior (*22*–*25*), we introduce here a smart and flexible skin with anisotropic frictional properties that enables a single soft actuator to propel itself. To this end, we took advantage of kirigami, the ancient Japanese art of paper cutting, whose principles have recently emerged as promising tools to realize highly stretchable and morphable structures (*26*–*29*). We realized the skin by embedding an array of properly designed cuts into a planar plastic sheet (Fig. 1A) and then wrapping it around a soft actuator (see Fig. 1, B to D). Upon inflation, the elongation of the actuator triggered a mechanical instability in the kirigami skin that in turn induced the pop-up of a three-dimensional (3D) morphology similar to that of a snake's skin (Fig. 1, E and F). The highly directional 3D features induced by buckling significantly altered the frictional properties of the kirigami skins and enabled our simple machine to move forward. The buckling-induced pop-up process observed in our kirigami skin resembles the ability of the snakes to actively actuate their scales (Fig. 1F and movie S1) to tune their frictional properties (*5*).

RESULTS

We considered a soft fluidic actuator comprising an elastomeric tube made of silicone rubber (Smooth-On Inc., Ecoflex 00-30; shear modulus $\mu_a \simeq 30$ kPa) with a length of 164 mm and a triangular cross section with edges of 25 mm (see Fig. 1, B and C). To maximize its elongation during inflation and constrain any other mode of deformation, we surrounded the tube with stiff Kevlar fibers arranged in a helical pattern with small pitch (so that the fibers were almost aligned with the circumferential direction—see the Supplementary Materials for details). We found that the actuator extended by 25% when inflated with a maximum volume of $V_{max} = 24$ ml of air. However, because symmetry resulted in equal movements of both actuator ends during inflation and deflation, this system did not move forward when placed on a substrate (see movie S2).

Next, we covered the actuator with kirigami skins (see Fig. 1D and movie S3) and investigated their effect on its ability to move. Our kirigami skins were fabricated by laser cutting 9 by 32 centimeter-scale unit cells arranged on a triangular lattice with spacing of $l = 4.5$ mm and hinge width of $\delta = 0.7$ mm into polyester plastic sheets (Artus Corporation; Young's modulus of $E = 4.33$ GPa, see fig. S2). Inspired by the shapes observed in ventral scales of snakes (*22*), we considered four different cuts (see Fig. 2A): (i) linear cuts, (ii) triangular cuts, (iii) circular cuts, and (iv) trapezoidal cuts. For all assembled kirigami-skinned crawlers, we first characterized their elongation (ε) and pressure (P) as a function of the supplied volume (V) and then investigated how inflation affected the frictional force when they moved on a substrate. To this end, we pulled (i.e., moved backward) and pushed (i.e., moved forward) the crawlers inflated by different amounts of air against a rough surface (polyurethane foam) while monitoring the resistive force (F_{fr}). Effective coefficients of friction in backward (μ_b) and forward (μ_f) directions were then extracted from these measurements as

$$\mu_b = \frac{\left\langle F_b^{peak} \right\rangle}{F_N}, \quad \mu_f = \frac{\left\langle F_f^{peak} \right\rangle}{F_N} \tag{1}$$

where $F_N \simeq 0.2$ N is the crawler's weight, $\langle \cdot \rangle$ denotes the mean value, and F_b^{peak} and F_f^{peak} are the local peaks of F_{fr} recorded during pulling and pushing, respectively (see the Supplementary Materials for details).

Although the pattern with linear cuts has been used frequently to design highly stretchable systems (*26*, *29*), we found that the corresponding kirigami skin severely limited the extensibility of the actuator [i.e., $\varepsilon = (L - L_0)/L_0 < 0.05$, L_0, and L denoting the undeformed and deformed lengths of the perforated part of the skin (Fig. 2B)] and made it very stiff (see Fig. 2C). This is because the antisymmetric out-of-plane buckling mode typical of this kirigami sheet is characterized by alternating up and down (see fig. S6B) buckled ligaments (*26*) and therefore is suppressed by the presence of the actuator. Hence, no features pop up upon inflation (see inset in Fig. 2F), the crawler slides

John A. Paulson School of Engineering Applied Sciences, Harvard University, Cambridge, MA 02138, USA.
*Corresponding author. Email: bertoldi@seas.harvard.edu

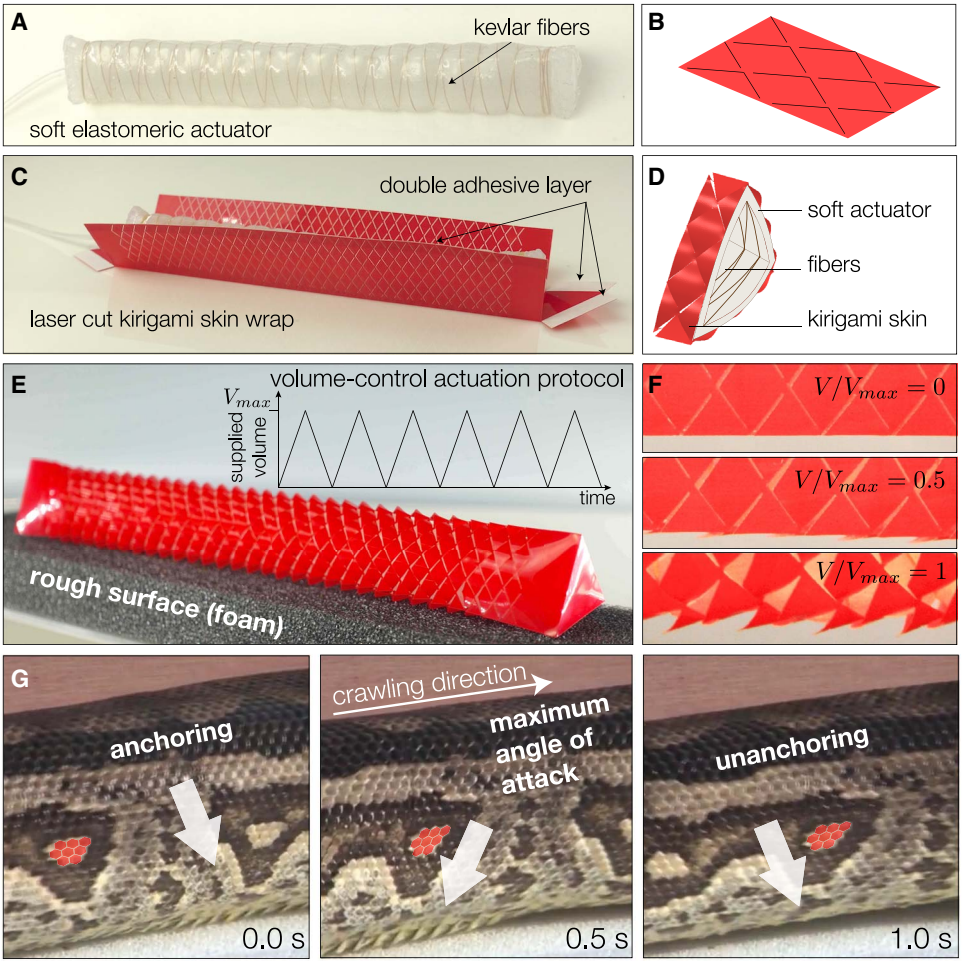

Fig. 1. Kirigami-skinned soft crawlers. (**A**) We considered a fiber-reinforced elastomeric soft actuator that extends axially upon inflation. (**B**) A kirigami skin was fabricated by embedding an array of cuts into a thin plastic sheet. (**C**) A kirigami-skinned soft crawler was built by wrapping the kirigami skin around the actuator. (**D**) Cross-sectional view of a kirigami-skinned soft crawler. (**E**) Inflation of the actuator resulted in a buckling-induced pop-up texture similar to that of a snake's skin. Inset: A typical volume-control actuation protocol with a maximum volume V_{max}. (**F**) Close-up views of a kirigami skin with triangular cuts at a different level of supplied volume V (note that V_{max} = 24 ml is the maximum supplied volume). (**G**) Snapshots showing the rectilinear gait of a female Dumeril's boa (*Acrantophis dumerili*). The snake actively tilts the ventral scales to increase frictional anisotropy and enhance anchoring (video courtesy of H. Marvi and D. Hu).

smoothly in both directions, and the frictional force recorded during pulling and pushing reaches similar values, which are not affected by the supplied volume V (see red lines in Fig. 2, D and E), yielding $\mu_f(V) \simeq \mu_b(V) \simeq 0.75 - 1$ (see Fig. 2F).

By contrast, we found that the other three skins only moderately limited the extensibility of the soft actuator (i.e., $\varepsilon \simeq 0.12 \sim 0.18$, see Fig. 2B) and resulted in a pressure-elongation curve characterized by an initial linear regime, a pressure plateau, and a final stiffening. While in the initial linear regime, all hinges bent in-plane, and the skins remained flat; the sudden departure from linearity to a plateau stress was caused by the out-of-plane buckling of the hinges, which induced the formation of a 3D pattern similar to that of a snake's skin with all features homogeneously popping outward (see insets in Fig. 2, G to I, and fig. S8). This buckling-induced pop-up significantly altered the measured frictional force. Before the instability (i.e., for supplied volume ratios $V/V_{max} < 0.25$), the crawlers slid smoothly in both forward and backward directions, and $\mu_b \simeq \mu_f \simeq 1 \sim 1.5$ for all three systems (the slight increase in μ_b and μ_f compared to the case of the skin with linear cuts was due to the sharper features of the cuts). However, above the instability threshold (i.e., for supplied volume ratios $V/V_{max} > 0.25$), the popping out of the features defined by the cuts led to a jerking motion in backward direction, with the crawlers that alternatively stuck to the substrate and slid over it. This stick-slip regime was also apparent from the measured frictional force, which presented a discrete sequence of sharp drops (see Fig. 2E). Moreover, the instability-induced pop-up process resulted in a significant increase of the magnitude of F_{fr} measured during pulling (see Fig. 2E) so that $\mu_b >> \mu_f$ for supplied volume ratios $V/V_{max} > 0.25$. Therefore, our results indicate that buckling can be exploited to transform the frictional properties of a surface from isotropic to highly anisotropic. However, for this transformation to happen, it is necessary that all features pop up in the same direction (i.e., toward the crawlers' tail). To demonstrate this important point, we considered a kirigami skin with half of the triangular cuts pointing to the head of the crawler and the remaining pointing to its tail (we refer to this pattern as the mirrored triangular pattern). In this case, buckling triggered a pop-up process, and the symmetry of the resulting 3D pattern induced a significant increase of both μ_f and μ_b and did not introduce any frictional directionality (i.e., $\mu_b \sim \mu_f$, see fig. S6C).

Having characterized the tribological behavior of our kirigami-skinned crawlers, we then investigated how friction affected their ability to crawl. To this end, we monitored the position of the crawlers placed on a rough surface (polyurethane foam) as they were inflated by supplying a volume of air V_{max} = 24 ml and deflated by extracting the same amount of fluid at a rate of 300 ml/min (see movie S4). In Fig. 3A, we overlay initial and final positions of the crawlers after six inflation cycles, whereas in Fig. 3B, we report the evolution of the displacement of their centers of mass (solid lines), tails (dashed lines), and heads (dotted lines). These results indicate that the crawlers with kirigami skins exhibiting directional frictional properties (i.e., those with circular, triangular, and trapezoidal cuts) were capable of propelling themselves much more efficiently than the other ones. Specifically, if we indicated with u_{cycle}, the displacement recorded at the end of each cycle, then we found that u_{cycle}/L_0 = 0, 0.015, 0.068, 0.08, and 0.12 for the kirigami-skinned crawlers with linear, mirrored triangular, triangular, circular, and trapezoidal cuts, respectively. Although the poor performance of the kirigami-skinned crawler with linear cuts can be attributed to its very limited extensibility, the very short distance traveled by the crawler

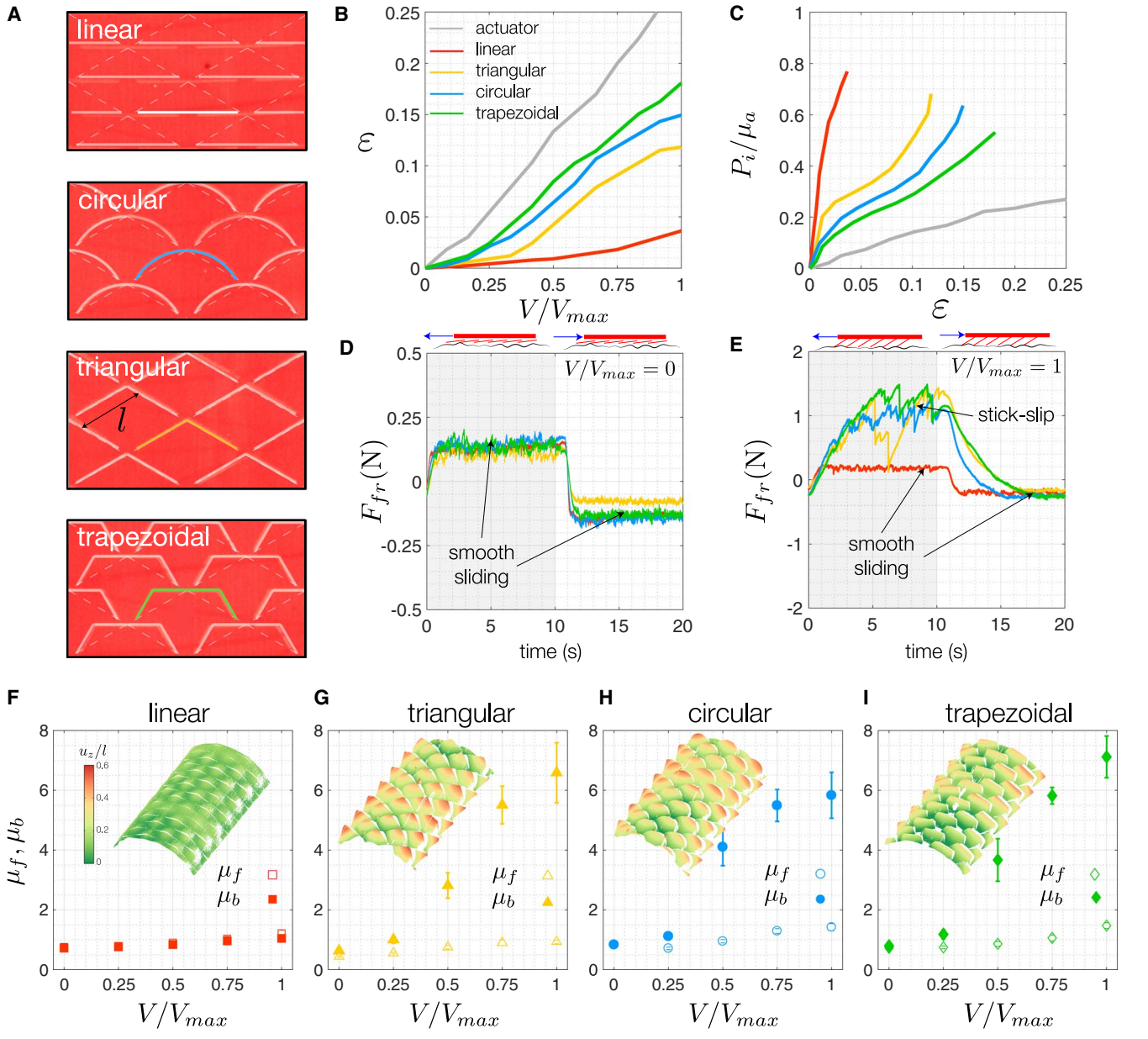

Fig. 2. Characterization of kirigami-skinned soft crawlers. (**A**) Cut shapes considered in this study. (**B**) Elongation of the crawlers as a function of their volume. (**C**) Pressure normalized by the shear modulus of actuator μ_a versus axial strain for the kirigami-skinned crawlers. (**D** and **E**) Friction force F_{fr} measured in backward and forward directions at supplied volumes (D) $V/V_{max} = 0$ and (E) $V/V_{max} = 1$ (with a maximum volume V_{max} = 24 ml). (**F** to **I**) Effective coefficients of friction versus inflation levels in forward (hollow symbols) and backward (filled symbols) directions with (F) linear, (G) triangular, (H) circular, and (I) trapezoidal cuts. Insets: 3D-scanned surface profiles of the skins at the supplied volume $V/V_{max} = 1$.

with the mirrored triangular cuts points to the importance of the anisotropic frictional properties introduced by the buckled kirigami skins. Last, we note that the efficiency of our kirigami-skinned crawlers with anisotropic frictional properties (i.e., those with triangular, circular, and trapezoidal cuts) was mainly determined by the stretchability of their skin. The skin with trapezoidal cuts was more stretchable than those with circular and triangular cuts and, therefore, enabled the crawler to have a longer stride and move further.

To further understand how the frictional properties of our kirigami skins affect locomotion, we focused on the position of the anchor point (x_a) at which the crawlers gripped the substrate (i.e., the instantaneous stagnation point along the crawler body) to pull themselves forward and prevent backward sliding (*6*). By balancing the frictional forces exerted by the substrate on the skin (while neglecting inertial forces due to the slow nature of the crawling motion), we show that (see the Supplementary Materials for details)

$$\left(\frac{x_a}{L}\right)_{\text{inflation}} = \frac{1}{2}\left(\frac{\mu_f - \mu_b}{\mu_f + \mu_b}\right), \quad \left(\frac{x_a}{L}\right)_{\text{deflation}} = \frac{1}{2}\left(\frac{\mu_b - \mu_f}{\mu_f + \mu_b}\right) \qquad (2)$$

which provides explicit relations between the position of the anchor point and the frictional properties of the kirigami skin. Equation 2

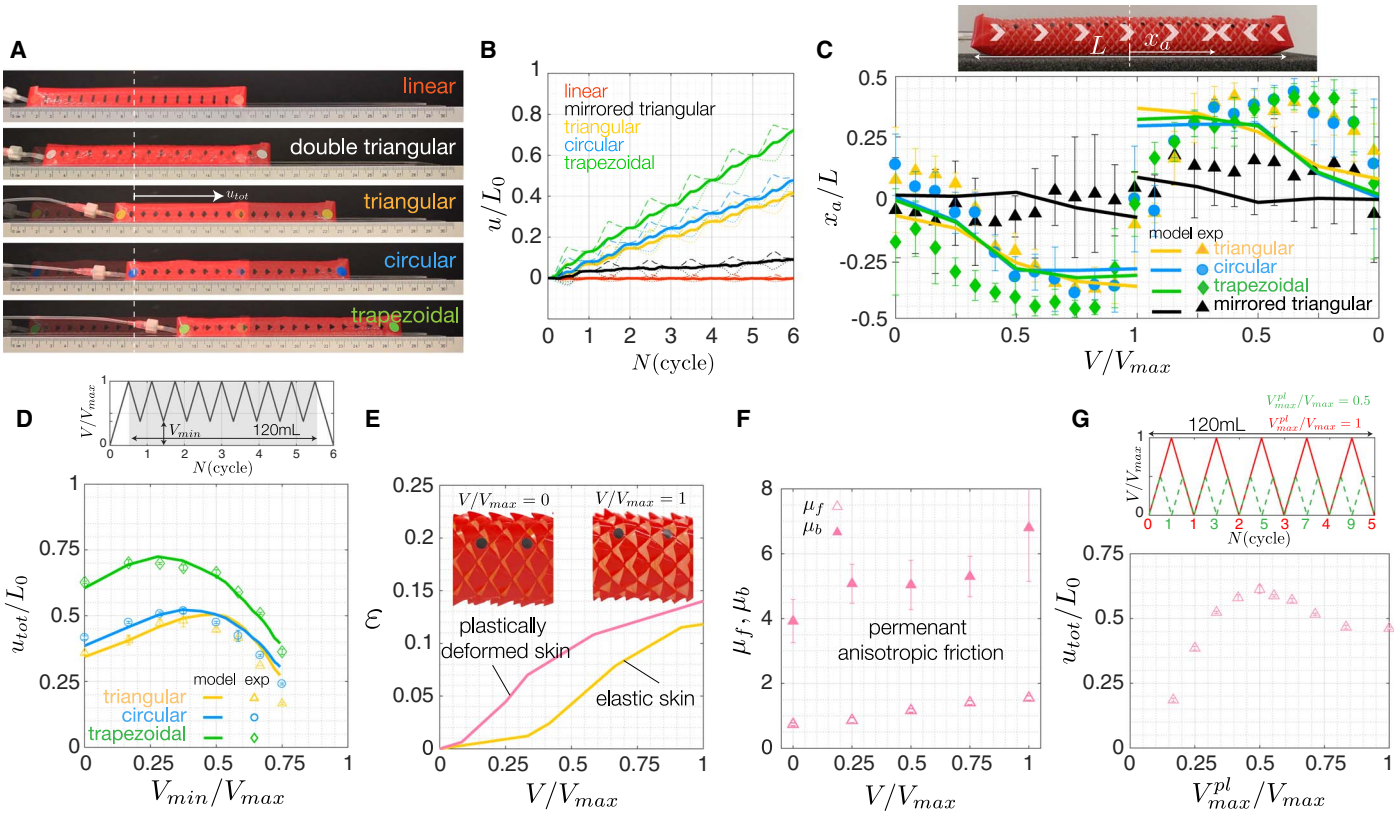

Fig. 3. Crawler locomotion. (**A**) Initial and final position of the crawlers after six inflation cycles with $V \in [0,24]$ ml. (**B**) Displacement of the center of mass (solid line), head (dashed line), and tail (dotted line) of the crawlers versus number of cycles. (**C**) Position of the anchor point during inflation and deflation. The markers denote the experimental data over six cycles. The solid lines denote the predictions given by Eq. 2 using the experimentally measured friction coefficients. (**D**) Measured (markers) and predicted (continuous lines) total displacement when a volume of 120 ml of air was supplied by cyclically inflating and deflating the actuators between V_{max} = 24 ml and $V_{min} \in [0,V_{max}]$. (**E**) Elongation versus supplied volume for a kirigami-skinned crawler with triangular cuts. Results for elastic (yellow line) and plastically deformed (purple line) skins are compared. The inset shows the plastically deformed skin at V/V_{max} = 0 and 1 (with V_{max} = 24 ml). (**F**) Effective coefficients of friction versus supplied volume for the crawler with the plastically deformed skin. (**G**) Measured total displacement for the crawler with the plastically deformed skin when a volume of 120 ml of air was supplied by cyclically inflating and deflating it between 0 ml and V^{pl}_{max}, with $V^{pl}_{max} \in [0,24]$ ml. Error bars indicate SD of the measured anchor points during six inflation/deflation cycles.

indicates that, to maximize the distance traveled by the crawlers, the ratio μ_b/μ_f should be as large as possible. In this case, x_a/L approaches ±0.5, and anchoring occurs at the tail during inflation/elongation and at the head during deflation/shortening, completely preventing backward sliding. Moreover, Eq. 2 also shows that for $\mu_b \sim \mu_f$, the anchor point is located at the center of mass of the crawlers (i.e., $x_a/L \sim 0$). In this case, the head and tail of the crawlers move by the same amount (but in opposite directions) during inflation and deflation, and there is no advancement. In Fig. 3C, we compared the position of the anchor point extracted by our tests with that predicted by Eq. 2 using the experimentally measured friction coefficients reported in Fig. 2 (F to I). We found that the trends observed in our experiments are well captured by our simple model. When the kirigami skin has isotropic frictional properties (as for the patterns with mirrored triangular cuts during the entire inflation/deflation process and with circular, triangular, and trapezoidal cuts before buckling), then x_a/L is about 0. By contrast, if $\mu_b >> \mu_f$ (as for the skins with triangular, circular, and trapezoidal cuts after buckling), then the anchor point moves toward the tail and the head of the crawler during inflation and deflation, respectively.

The results reported in Fig. 3 (A to C) show that, by taking advantage of the directional frictional properties induced in the kirigami skins by buckling, even a single soft actuator can propel itself. They also indicate that the conditions used in our experiments were not optimal, because even for our best kirigami-skinned crawlers, the anchor points were located near their centers of mass for volume ratios $V/V_{max} < 0.25$. This limitation can be overcome by not fully deflating the actuators so that they always operate in the region where the skin has anisotropic frictional properties. In Fig. 3E, we report the measured (markers) and predicted (continuous lines) total displacement (u_{tot}) when a total volume V_{tot} = 120 ml of air was supplied by cyclically inflating and deflating them between the maximum volume V_{max} = 24 ml and the minimum volume $V_{min} \in [0,V_{max}]$ (see movie S5 and the Supplementary Materials for details). We found that there is an optimum value of the minimum volume V_{min} for which the crawlers move more efficiently. Whereas for smaller values of the minimum volume V_{min}, the lack of anisotropic frictional properties resulted in smaller total displacement u_{tot}, when V_{min} was increased above the optimum value, the limited change in length experienced by the crawlers during the cycles became the limiting factor.

To date, we have considered kirigami skins that were initially flat and in which buckling induced the reversible and repeatable formation of a 3D directional texture, but plastic deformation at the ligaments can also be harnessed to generate a permanent 3D morphology

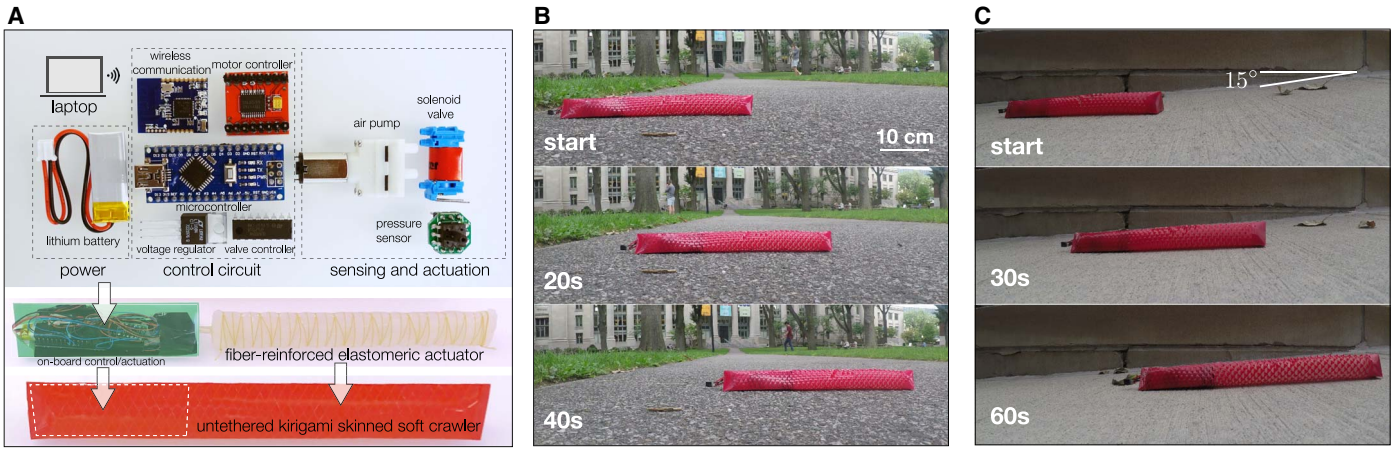

Fig. 4. Untethered kirigami-skinned soft crawlers. (**A**) Fabrication of our untethered kirigami-skinned crawlers. (**B**) Untethered kirigami-skinned soft crawler with circular cuts moves over asphalt. (**C**) Untethered kirigami-skinned soft crawler with trapezoidal cuts climbs a concrete ramp.

(*28*) and, therefore, to improve the efficiency of the crawlers. To demonstrate this, we considered a kirigami skin with triangular cuts, and before wrapping it around the actuators, we applied a large stretch so that in the post-buckling regime, plastic strains developed in the ligament between the cuts, creating a permanent pop-up pattern (see insets of Fig. 3E). We found that this plastically deformed skin affected the response of the system in two ways. On the one hand, it increased the elongation that the crawler experienced at the beginning of the inflation process (Fig. 3E). On the other hand, its permanent directional texture resulted in highly anisotropic frictional properties through the entire actuation process (Fig. 3F). Hence, the efficiency in locomotion for this crawler was optimal when the supplied volume was cyclically varied between 0 and 12 ml (Fig. 3G), resulting in ~22% improvement in comparison to the best performance of the corresponding crawler with a purely elastic kirigami skin.

CONCLUSION

In summary, we have demonstrated that kirigami principles can be exploited to create bioinspired flexible and morphable skins with directional frictional properties that can be integrated in soft robots to achieve locomotion even with a single extending actuator. Although several techniques (including rapid prototyping, pop-up fabrication, and origami) have been proposed to fabricate morphable structures in the recent years, we believe that the proposed kirigami approach provides a simpler, faster, and cheaper technique to create them. Our kirigami skins were fabricated by simply embedding an array of cuts into a planar thin sheet. Mechanical instabilities triggered under uniaxial tension were then exploited to create a 3D pattern and even to guide the formation of permanent folds.

We have shown that the efficiency of our kirigami-skinned crawlers can be improved by properly balancing the frictional properties and stretchability of the skins through careful choice of the cut geometry and the actuation protocol. Moreover, our results indicate that the plastic deformation at the hinges can be harnessed to further optimize the response of the system. However, the reversible and repeatable pop-up process observed in the elastic regime offers opportunities for on-demand and active control of friction, which is important for a broad range of applications, including robotic manipulation and transfer printing (*23*). Although we have focused on fluid-driven soft actuators in this study, the designed stretchable kirigami skins can also be applied to different classes of soft robots, including those based on dielectric elastomers (*30*, *31*), shape memory polymers (*32*), shape memory alloys (*15*, *20*, *21*), and hydrogels (*33*). In addition, because the properties of the designed kirigami skins are primarily governed by the geometry of the structure rather than the constitutive properties of the material, the proposed principles can be applied to systems over a wide range of length scales and made of different materials. Hence, recent advances in top-down techniques, such as photolithography (*26*), open up exciting opportunities for miniaturization of the proposed architectures. On the other side, thicker and stiffer sheets can be used to realize skins for larger robots such as planetary rovers for space exploration.

Last, we note that all crawlers considered in this study were actuated pneumatically using air transferred to them from a stationary source via a flexible tube. However, real-world applications require systems that are capable of operating without the constraint of a tether. As a first step in this direction, we built a fully untethered kirigami-skinned soft crawler by integrating on-board control, sensing, actuation, and power supply (Fig. 4A, see the Supplementary Materials for details). Because all these components can be packed into a volume as small as 25 mm^3 and as light as 45 g, they can be attached to the tail of the actuator without limiting its ability to move on a variety of terrains (Fig. 4, B and C, movies S6 to S10, and fig. S13). Hence, we believe that our kirigami-based strategy opens avenues for the design of new class of soft crawlers that can travel across complex environments for search and rescue, exploration and inspection operations, environmental monitoring, and medical procedures.

MATERIALS AND METHODS

Fabrication of kirigami-skinned crawlers

The kirigami-skinned soft crawlers investigated in this study comprised a fiber-reinforced soft actuator wrapped with a kirigami sheet. The fiber-reinforced soft actuators were made by pouring a platinum-catalyzed silicone rubber (Ecoflex 00-30, Smooth-On Inc.) into a 3D-printed mold. The actuator has a hollow prismatic tube with a triangular cross section. To maximize the elongation of the actuator upon inflation and constrain its deformation in the circumferential direction, we surrounded the elastomeric tube by stiff Kevlar fibers arranged in a helical pattern. The fibers were held in place by brushing the surface

of the actuator with a very thin layer of uncured elastomer. The kirigami skins were fabricated by laser cutting an array of 9 by 32 unit cells into 51-μm thick polyester plastic sheets (Artus Corporation, NJ). To assemble the kirigami-skinned crawlers, we wrapped the kirigami sheet around the fiber-reinforced actuator and attached its two edges together using a double-sided adhesive sheet (Blick Art Materials, IL). More details on crawler design, geometry of cuts, fabrication, testing methods, analytical model, and finite-element simulations may be found in the Supplementary Materials.

SUPPLEMENTARY MATERIALS

robotics.sciencemag.org/cgi/content/full/3/15/eaar7555/DC1
Supplementary sections S1 to S4.
Fig. S1. Fabrication of an extending fiber-reinforced actuator.
Fig. S2. Kirigami patterns.
Fig. S3. Fabrication and assembly of kirigami-skinned crawlers.
Fig. S4. Untethered kirigami-skinned crawler.
Fig. S5. Mechanical response of the actuator.
Fig. S6. Mechanical response of kirigami sheets.
Fig. S7. Mechanical response of kirigami-skinned crawlers.
Fig. S8. Evolution of surface morphology for our kirigami-skinned crawlers.
Fig. S9. Friction measurement setup.
Fig. S10. Friction measurements.
Fig. S11. Effective friction coefficients.
Fig. S12. Frictional properties of a crawler with a plastically deformed skin.
Fig. S13. Locomotion of our untethered kirigami-skinned crawler.
Fig. S14. Relation between the location of the anchor point and the fraction coefficients.
Fig. S15. Finite-element simulations of kirigami unit cells.
Movie S1. Rectilinear gait of a female Dumeril's boa.
Movie S2. A fiber-reinforced extending actuator is placed over a rough surface and is subjected to cyclic inflation/deflation.
Movie S3. Assembly of a kirigami-skinned soft crawler.
Movie S4. Motion of the crawlers during six inflation cycles with $V \in [0,24]$ ml.
Movie S5. Motion of the crawlers when a total volume V_{tot} = 120 ml of air is supplied by cyclically inflating and deflating them between V_{max} = 24 ml and $V_{min} \in [0,V_{max}]$.
Movie S6. Fully untethered kirigami skinned crawlers with triangular, circular, and trapezoidal kirigami skins.
Movie S7. An untethered crawler with circular kirigami skin propels itself over asphalt.
Movie S8. An untethered crawler with trapezoidal kirigami skin climbs a concrete ramp.
Movie S9. An untethered crawler with triangular kirigami skin propels itself over rough stone.
Movie S10. Motion of an untethered crawler with trapezoidal kirigami skin for P_{min} = 1, 4, 8, and 12 kPa and P_{max} = 16 kPa.
References (*34*–*38*)

REFERENCES AND NOTES

1. H. W. Lissmann, Rectilinear locomotion in a snake (*Boa occidentalis*). *J. Exp. Biol.* **26**, 368–379 (1950).
2. M. Denny, Locomotion: The cost of gastropod crawling. *Science* **208**, 1288–1290 (1980).
3. D. Berrigan, D. J. Pepin, How maggots move: Allometry and kinematics of crawling in larval Diptera. *J. Insect Physiol.* **41**, 329–337 (1995).
4. R. D. Maladen, Y. Ding, C. Li, D. I. Goldman, Undulatory swimming in sand: Subsurface locomotion of the sandfish lizard. *Science* **325**, 314–318 (2009).
5. H. Marvi, J. P. Cook, J. L. Streator, D. L. Hu, Snakes move their scales to increase friction. *Biotribology* **5**, 52–60 (2016).
6. R. M. Alexander, *Principles of Animal Locomotion* (Princeton Univ. Press, 2006).
7. D. L. Hu, J. Nirody, T. Scott, M. J. Shelley, The mechanics of slithering locomotion. *Proc. Natl. Acad. Sci. U.S.A.* **106**, 10081–10085 (2009).
8. J. Hazel, M. Stone, M. S. Grace, V. V. Tsukruk, Nanoscale design of snake skin for reptation locomotions via friction anisotropy. *J. Biomech.* **32**, 477–484 (1999).
9. R. A. Berthé, G. Westhoff, H. Bleckmann, S. N. Gorb, Surface structure and frictional properties of the skin of the Amazon tree boa *Corallus hortulanus* (Squamata, Boidae). *J. Comp. Physiol. A* **195**, 311–318 (2009).
10. D. Trivedi, C. D. Rahn, W. M. Kier, I. D. Walker, Soft robotics: Biological inspiration, state of the art, and future research. *Appl. Bionics Biomech.* **5**, 99–117 (2008).
11. C. Majidi, Soft Robotics: A perspective–current trends and prospects for the future. *Soft Robotics* **1**, 5–11 (2013).
12. S. Kim, C. Laschi, B. Trimmer, Soft robotics: A bioinspired evolution in robotics. *Trends Biotechnol.* **31**, 287–294 (2013).
13. D. Rus, M. T. Tolley, Design, fabrication and control of soft robots. *Nature* **521**, 467–475 (2015).
14. N. W. Pikul, S. Li, H. Bai, R. T. Hanlon, I. Cohen, R. F. Shepherd, Stretchable surfaces with programmable 3D texture morphing for synthetic camouflaging skins. *Science* **358**, 210–214 (2017).
15. A. Menciassi, D. Accoto, S. Gorini, P. Dario, Development of a biomimetic miniature robotic crawler. *Auton. Robotics* **21**, 155–163 (2006).
16. J. Z. Ge, A. A. Calderón, N. O. Pérez-Arancibia, An earthworm-inspired soft crawling robot controlled by friction. arXiv 1707.04084 (2017).
17. K. Suzumori, T. Hama, T. Kanda, New pneumatic rubber actuators to assist colonoscope insertion, in *IEEE International Conference on Robotics and Automation*, (ICRA, 2006), pp. 1824–1829.
18. R. F. Shepherd, F. Ilievski, W. Choi, S. A. Morin, A. A. Stokes, A. D. Mazzeo, X. Chen, M. Wang,G. M. Whitesides, Multigait soft robot. *Proc. Natl. Acad. Sci. U.S.A.* **108**, 20400–20403 (2011).
19. F. Connolly, P. Polygerinos, C. J. Walsh, K. Bertoldi, Mechanical programming of soft actuators by varying fiber angle. *Soft Robotics* **2**, 26–32 (2015).
20. S. Seok, C. Denizel Onal, K.-J. Cho, R. J. Wood, D. Rus, S. Kim, Meshworm: A peristaltic soft robot with antagonistic nickel titanium coil actuators. *IEEE/ASME Trans. Mechatronics* **18**, 1485–1497 (2013).
21. T. Umedachi, V. Vikas, B. A. Trimmer, Softworms: The design and control of non-pneumatic, 3D-printed, deformable robots. *Bioinspir. Biomim.* **11**, 025001 (2016).
22. H. A. Abdel-Aal, M. El Mansori, Tribological analysis of the ventral scale structure in a *Python regius* in relation to laser textured surfaces. *Surf. Topogr. Metrol. Prop.* **1**, 015001 (2013).
23. H. Marvi, Y. Han, M. Sitti, Actively controlled fibrillar friction surfaces. *Appl. Phys. Lett.* **106**, 051602 (2015).
24. S. Das, N. Cadirov, S. Chary, Y. Kaufman, J. Hogan, K. L. Turner, J. N. Israelachvili, Stick–slip friction of gecko-mimetic flaps on smooth and rough surfaces. *J. R. Soc. Interface* **12**, 20141346 (2015).
25. T. Yamaguchi, Y. Sawae, S. M. Rubinstein, Effects of loading angles on stick–slip dynamics of soft sliders. *Extreme Mech. Lett.* **9**, 331–335 (2016).
26. T. C. Shyu, P. F. Damasceno, P. M. Dodd, A. Lamoureux, L. Xu, M. Shlian, M. Shtein, S. C. Glotzer, N. A. Kotov, A kirigami approach to engineering elasticity in nanocomposites through patterned defects. *Nat. Mater.* **14**, 785–789 (2015).
27. M. K. Blees, A. W. Barnard, P. A. Rose, S. P. Roberts, K. L. McGill, P. Y. Huang, A. R. Ruyack, J. W. Kevek, B. Kobrin, D. A. Muller, P. L. McEuen, Graphene kirigami. *Nature* **524**, 204–207 (2015).
28. A. Rafsanjani, K. Bertoldi, Buckling-induced kirigami. *Phys. Rev. Lett.* **118**, 084301 (2017).
29. Y. Tang, G. Lin, S. Yang, Y. K. Yi, R. D. Kamien, J. Yin, Programmable kiri-kirigami metamaterials. *Adv. Mater.* **29**, 1604262 (2017).
30. S. Shian, K. Bertoldi, D. R. Clarke, Dielectric elastomer based "grippers" for soft robotics. *Adv. Mater.* **27**, 6814–6819 (2015).
31. T. Li, G. Li, Y. Liang, T. Cheng, J. Dai, X. Yang, B. Liu, Z. Zeng, Z. Huang, Y. Luo, T. Xie, W. Yang, Fast-moving soft electronic fish. *Sci. Adv.* **3**, e1602045 (2017).
32. A. Miriyev, K. Stack, H. Lipson, Soft material for soft actuators. *Nat. Commun.* **8**, 596 (2017).
33. H. Yuk, S. Lin, C. Ma, M. Takaffoli, N. X. Fang, X. Zhao, Hydraulic hydrogel actuators and robots optically and sonically camouflaged in water. *Nat. Commun.* **8**, 14230 (2017).
34. B. C. Jayne, S. J. Newman, M. M. Zentkovich, H. M. Berns, Why arboreal snakes should not be cylindrical: Body shape, incline and surface roughness have interactive effects on locomotion. *J. Exp. Biol.* **218**, 3978–3986 (2015).
35. F. Connolly, C. J. Walsh, K. Bertoldi, Automatic design of fiber-reinforced soft actuators for trajectory matching. *Proc. Natl. Acad. Sci. U.S.A.* **114**, 51–56 (2017).
36. A. Lamoureux, K. Lee, M. Shlian, S. R. Forrest, M. Shtein, Dynamic kirigami structures for integrated solar tracking. *Nat. Commun.* **6**, 8092 (2015).
37. M Isobe, K. Okumura, Initial rigid response and softening transition of highly stretchable kirigami sheet materials. *Sci. Rep.* **6**, 24758 (2016).
38. M. Senn, C. Eberl, Digital Image Correlation and Tracking (2015); https://uk.mathworks.com/matlabcentral/fileexchange/50994-digital-imagecorrelation-and-tracking.

Acknowledgments
Funding: Research was supported by the NSF under grant number DMR-1420570. A.R. acknowledges the financial support provided by the Swiss National Science Foundation under grant number P300P2-164648. **Author contributions:** A.R. and K.B. conceived the concepts and designed the research. A.R., Y.Z., and B.L. built the crawlers and performed the experiments. B.L. developed the control unit for the untethered crawler. A.R. and S.M.R developed the theoretical model. A.R., S.M.R., and K.B. analyzed the data and wrote the paper.

K.B. supervised the research. **Competing interests:** A.R. and K.B. are named inventors on U.S. Provisional Patent Application No. 62,624,371, which has been submitted by President and Fellows of Harvard College and generally covers transformation of a 2D sheet into a 3D-patterned, perforated surface, such as a kirigami structure induced by buckling of interconnecting ligaments. The other authors declare no competing interests. **Data and materials availability:** All data needed to support the conclusions are in the main text or the Supplementary Materials.

Submitted 13 December 2017
Accepted 2 February 2018
Published 21 February 2018
10.1126/scirobotics.aar7555

Citation: A. Rafsanjani, Y. Zhang, B. Liu, S. M. Rubinstein, K. Bertoldi, Kirigami skins make a simple soft actuator crawl. *Sci. Robot.* **3**, eaar7555 (2018).

Science Robotics

Kirigami skins make a simple soft actuator crawl

Ahmad Rafsanjani, Yuerou Zhang, Bangyuan Liu, Shmuel M. Rubinstein, and Katia Bertoldi

Sci. Robot. **3** (15), eaar7555. DOI: 10.1126/scirobotics.aar7555

Science Robotics (ISSN 2470-9476) is published by the American Association for the Advancement of Science. 1200 New York Avenue NW, Washington, DC 20005. The title *Science Robotics* is a registered trademark of AAAS.